ARCHIVES OF ACOUSTICS
22, 3, 307–331 (1997)

MATCHED ALL-PASS FILTERING OF THE RECEIVED ECHOES FOR RANGE IMPROVEMENT IN MEDICAL ULTRASOUND IMAGING

A. NOWICKI, A. KUBERA, K. RENE

Department of Ultrasound,
Institute of Fundamental Technological Research,
Polish Academy of Sciences
(00-049 Warszawa, ul. Świętokrzyska 21)

P.A. LEWIN

Drexel University, Philadelphia, USA

T. PAŁKO

Warsaw University of Technology, Warsaw, Poland

The purpose of this work was to investigate a possibility of using chirp waveforms in very high frequency ultrasound medical imaging to increase range resolution and concurrently maximize penetration depth. It is shown that the improvement in range resolution can be achieved by using appropriately designed all pass matched filter at the receiver input. The paper describes in depth theoretical optimization process and computer simulation of the matched 96-th order all pass filter for chirp waveforms of 1 μs duration in the frequency range 30 MHz – 50 MHz. A prototype of 24-th order filter was constructed to verify the results of analytical and numerical methods. Excellent agreement was observed between the theoretical predictions and experimental data. Continuation of this work will include design and optimization of superwide bandwidth transducers.

1. Introduction

Ultrasound imaging systems are widely used in clinical practice. For imaging of internal organs of human body frequencies from 2 MHz to about 12 MHz are applied. The range or axial resolution in tissue is determined by the duration of the ultrasound waveform launched into the body. Typically, the waveform contains two and a half periods, which leads to axial resolution of approximately 2 mm at the frequency of 2 MHz. Although at 10 MHz the resolution improves to 0.4 mm with increasing frequency, tissue attenuation also increases which, in turn, limits the penetration depth. Thus, while at

2 MHz the penetration depth may be on the order of tens of centimeters it decreases to tens of millimeters at 10 MHz.

Recently, very high frequency ultrasound imaging gained attention in surface tissue imaging and intraluminal examination of vessel walls [1, 2, 7, 13]. YANO *et al.* [15] were among the first researchers to describe a system permitting skin imaging using a 40 MHz lithium niobate transducer. They reported a – 6 dB beamwidth of about 0.1 mm in the focal zone. The axial resolution, determined from measurements of the length of a pulse reflected from an ideal reflector, was equal to 0.25 mm.

Several research groups used imaging transducers made of piezoelectric polivinylidene (di)fluoride (PVDF). Although PVDF suffers from a relatively low pulse-echo sensitivity in comparison with the conventional PZT piezoelectric ceramics (PVDF's electroacoustic coupling coefficient k_t is approx. 0.15 versus 0.5 for a conventional PZT ceramic material) it allows extremely wide bandwidth to be achieved, thus permitting the use of excitation signals with varying frequency. HOSS, EMERT *et al.* [8] described an imaging system with a pulse-echo PVDF transducer working at the centre frequency of 40 MHz and having −6 dB bandwidth of about 50 MHz. They have overcome the issue of low PVDF transducer sensitivity by employing chirp modulation as an excitation waveform and reported a significant increase in the overall imaging sensitivity. Chirped PVDF transducers were also studied by LEWIS [12]. BERSON *et al.* [2] described an ultrasound scanner operating at the center frequency of 47 MHz with axial resolution of about 0.1 mm and lateral resolution of 0.3 mm. FEUILLARD *et al.* [5] improved Berson's system replacing a PZT ceramic transducer by a broadband 45 MHz co-polymer transducer made of P(VDF-TrFe).

It is well known that range resolution can be improved by using chirp waveforms in which instantaneous frequency content changes as a function of elapsed time. Such waveforms with linear frequency modulation are widely used in the radar technique. By appropriately selecting duration of the waveform and modulation band and applying (e.g. surface acoustic wave) delay filters, both the resolution and range of the radar system can be enhanced [4, 6, 9, 14].

In medical ultrasound imaging the range resolution and penetration depth depend on the type of the interrogating waveform and processing of the returning echoes. Penetration depth can be improved by increasing the signal-to-noise ratio at the receiver output. However, for a given receiver noise level, such improvement requires increased energy level of the interrogating waveform. In practice, this can be achieved only by extending the pulse duration of transmitted waveforms as their peak amplitude is usually limited either by transmitter electronics or safety regulations [10]. The range resolution increases with decreasing duration of the echoes. In traditional pulse-echo ultrasound imaging it is well known that two objects can be distinguished if their respective echoes are separated by a time longer than the length of the interrogated waveforms. Thus, in conventional medical ultrasound imaging systems there is a clear trade-off between the range resolution and penetration depth. For the purpose of the discussion which follows it may be useful to note that the minimum distinguishable distance ΔR between neighbouring structures is defined as $\Delta R(c/2\Delta F)$, where c is the ultrasonic wave propagation velocity in the medium (tissue) and ΔF is the frequency bandwidth of the transmitted

signal. Thus, the 20 MHz bandwidth would correspond to the resolution in soft tissue ($c = 1540\,\mathrm{m/s}$) on the order of 0.04 mm.

The primary purpose of the work presented here was to investigate the conditions for simultaneous optimization of range (axial) resolution and penetration depth in very high frequency ultrasound medical imaging. The approach proposed uses chirp waveforms. As mentioned above such waveforms involve signals in which instantaneous frequency content changes as a function of elapsed time and can be considered as frequency modulated signals. The optimal use of chirp signals involves a form of echo compression techniques. HOSS *et al.* [8] reported application of similar signals in diagnostic ultrasound applications. However, their study did not discuss the issues involved in designing special receiver filters which would ensure echo compression by filter matching.

This paper is organized in the following way: In section 2 the theoretical background of echo compression technique using all pass matching filtering is outlined. Section 3 describes computer simulations and numerical solutions which allow optimizing of 96-th order filter. Experimental results obtained by testing a prototype of 24-th order filter are presented in Sec. 4. The theoretical and experimental results are compared in Sec. 5 which also contains conclusions and indicate the future work needed to further improve the proposed approach.

2. Theory of echo compression with frequency modulation using all-pass matching filtering

In this section theoretical analysis of ultrasound echo compression for transmitted waveforms with linear frequency modulation (chirps) is presented. The frequency spectrum of the chirp signal $s(t)$ considered has an almost rectangular envelope in the band ΔF around the centre frequency f_0. Such a chirp of duration T in which the frequency $f(t)$ varies linearly as a function of time, can be analytically expressed as:

$$s(t) = A\cos[f(t)], \tag{2.1}$$

where

$$f(t) = \begin{cases} \left(f_0 - \dfrac{\Delta F}{2}\right) + \dfrac{\Delta F}{T}t & \text{for} \quad 0 < t < T, \\ 0 & \text{for} \quad |t| > T. \end{cases}$$

As already mentioned the main advantage of using a chirp signal is that it enhances penetration depth by increasing the energy of the transmitted ultrasound wave providing that the echoes returning from the organs under examination are time compressed. This can be conveniently achieved by applying all pass (AP) matched filter approach to obtain pulse compression [3]. This technique involves implementation of a time dependent delay of the frequency components of the returning echoes. The delay increases linearly with increasing frequency of the individual components of the echo. The amplitude response of the AP filters is constant over the frequency bandwidth, i.e. signals with different frequency components are transferred by a filter with identical attenuation. The AP filters are ideally suited to implement specific delays, e.g. a constant delay or one which varies

linearly, over a given frequency range. As implied above, the use of pulse compression technique requires a filter with a linear delay. Both compression and decompression can be performed using the same AP filters [3].

Transfer characteristics of all-pass filters. Any overall characteristic of AP filters can be implemented by cascade connection of AP filters of the first and second orders. This can easily be shown by considering the following transformations.

The transfer function of the nth-order AP filter can be represented as:

$$H(s) = \frac{s^n + \beta_1 s^{n-1} + ... + \beta_n}{s^n + \alpha_1 s^{n-1} + ... + \alpha_n}, \tag{2.2}$$

where $s = j\omega$ and the coefficients α_n and β_n at the successive powers are real.

If $H(s)$ polynomial represents an AP type filter the poles and zeros of this function must follow a specific pattern. For the first order filter a pole and zero are located at equal distances from the origin. The pattern of the second order filter is often referred to as having quadrantal symmetry; here the poles and zeroes have equal but opposite real and imaginary parts (complex conjugate pattern). The patterns of higher order filters can be composed by a superposition of first and second order patterns.

Assuming that all the poles and zeros of $H(s)$ are complex conjugate except for one real pole and one real zero, the function $H(s)$ can be represented in the following way:

$$H(s) = \frac{s - \alpha_1}{s + \alpha_1} \times \frac{(s - \alpha_2)^2 + \beta_2^2}{(s + \alpha_2)^2 + \beta_2^2} \times ... \times \frac{(s - \alpha_{(n+1)/2})^2 + \beta_{(n+1)/2}^2}{(s + \alpha_{(n+1)/2})^2 + \beta_{(n+1)/2}^2}, \tag{2.3}$$

i.e., in this representation, $H(s)$ is the product of first- and second-order functions only. Such representation of the transfer function can always be obtained for AP filters with real coefficients at the successive powers of s. As mentioned above, in practice, $H(s)$ can be implemented by a cascade connection of AP filters of the first and second orders. In such implementation the total delay corresponds to the sum of the delays associated with individual filter sections. The cascade connection can be implemented since the individual sections exhibit constant electrical resistance. More specifically, the value of the input impedance of the filters is constant irrespective of the frequency. Higher order sections are seldom implemented because the savings in terms of the number of individual sections or components are negligible in comparison with the increased complexity of the filter and difficulties involved in its tuning.

In this work it was assumed that a filter with the appropriate phase delay function can be implemented by a cascade connection of the second order filters. The corresponding transfer function $H(s)$ is given by equation (2.4).

$$H(s) = \frac{(s - \alpha_2)^2 + \beta_2^2}{(s + \alpha_2)^2 + \beta_2^2} \times ... \times \frac{(s - \alpha_{(n+1)/2})^2 + \beta_{(n+1)/2}^2}{(s + \alpha_{(n+1)/2})^2 + \beta_{(n+1)/2}^2}. \tag{2.4}$$

Second-order all-pass filters. The transfer function of a second-order AP filter has the following form:

$$H_2(s) = \frac{(s - \alpha)^2 + \beta^2}{(s + \alpha)^2 + \beta^2}, \qquad \alpha > 0. \tag{2.5}$$

The delay function or phase response of the filter as a function of frequency is given by:

$$\theta_2(\omega) = -2\tan^{-1}\frac{2\alpha\omega}{\alpha^2+\beta^2-\omega^2}. \tag{2.6}$$

Therefore, the group delay function can be expressed as:

$$D_2(\omega) = -\frac{d\theta_2}{d\omega} = \frac{4\alpha(\omega^2+\alpha^2-\beta^2)}{(\alpha^2+\beta^2-\omega^2)^2+4\alpha^2\omega^2}. \tag{2.7}$$

It is more convenient to compare the behaviour of the function $D_2(\omega)$ for different values of α and β by introducing new variables:

$$\begin{aligned} \overline{\omega}_0^2 &= \alpha^2+\beta^2, \\ k &= \frac{2\alpha}{\overline{\omega}_0}, \\ \mu &= \frac{\omega}{\overline{\omega}_0}, \\ \alpha &= \frac{k\overline{\omega}_0}{2}, \\ \beta &= \overline{\omega}_0\sqrt{1-\frac{k^2}{4}}. \end{aligned} \tag{2.8}$$

where $\overline{\omega}_0$ – the normalized frequency, μ – the relative frequency.

Now the phase response of the filter can be expressed as:

$$\theta_2(\mu) = -2\tan^{-1}\frac{k\mu}{1-\mu^2}. \tag{2.9}$$

For $\mu = 0$, $(\omega = 0)$, the phase displacement is one of zero degrees and reaches 360° for the "infinite" frequency. The phase is 180° for $m = 1$ $(\omega = \omega_0)$ for all values of k.

With the new variables the group delay function is given by:

$$\overline{\omega}_0 D_2(\mu) = \frac{2k(1+\mu^2)}{(1-\mu^2)^2+k^2\mu^2}. \tag{2.10}$$

This function is shown in Fig. 1. The low values of k result in a narrow delay function with relatively large peak values. With increasing values of k the corresponding peak values decrease. For $k = 1.73$ the peak vanishes and the function is maximally flat for the angular frequency $\omega = 0$.

The impulse response of the matched filter for to the input signal $s(t)$ has the form:

$$h(t) = \begin{cases} \dfrac{2\sqrt{D}}{T}\cos\left(\omega_0 t - \dfrac{\Delta\omega}{2T}t^2\right) & -\dfrac{T}{2} \le t \le \dfrac{T}{2}, \\ 0 & |t| > \dfrac{T}{2}, \end{cases} \tag{2.11}$$

where $\omega_0 = 2\pi f_0$, $\Delta\omega = 2\pi\Delta F$.

The response $h(t)$ is characteristic of the non-causal system as the impulse response exists for negative time. To some extent, this facilitates the analysis since the filter

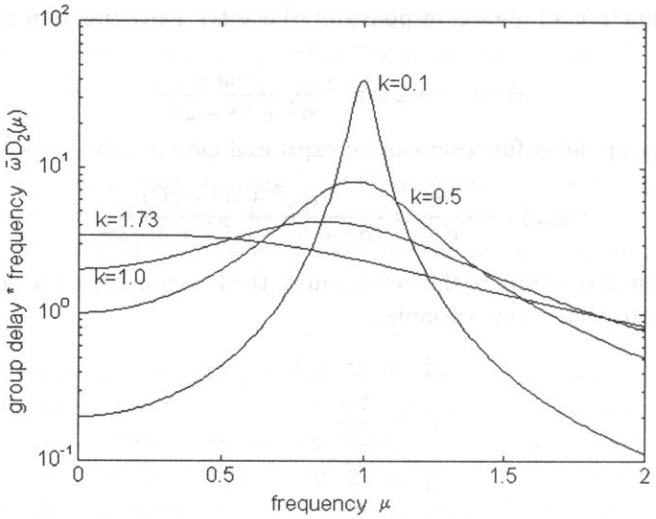

Fig. 1. The group delay function of the second-order filter.

response to the signal $s(t)$ is symmetrical with respect to $t = 0$. As evidenced later the filter implemented in practice shows an impulse response with an initial delay t_1.

The response of the matched filter to the signal $s(t)$ is given by the convolution integral:

$$y(t) = \frac{2\sqrt{D}}{T} \int_{-\infty}^{\infty} \cos\left(\omega_0\tau + \frac{\Delta\omega\tau^2}{2T}\right) \cos\left[\omega_0(t-\tau) - \frac{\Delta\omega}{2T}(t-\tau)^2\right] d\tau. \tag{2.12}$$

The integration limits can be conveniently defined considering a graphic interpretation of the convolution integral and bearing in mind that the response $h(t)$ precedes the one at the input (at time t_0) by the time $T/2$. After a few transformations the following expression can be obtained:

$$y(t) = \begin{cases} \dfrac{\sqrt{D}}{T} \displaystyle\int_{-T/2}^{t+T/2} P_1(t,\tau)\, d\tau + \dfrac{\sqrt{D}}{T} \int_{-T/2}^{t+T/2} P_2(t,\tau)\, d\tau & t < 0, \\ \dfrac{\sqrt{D}}{T} \displaystyle\int_{t-T/2}^{T/2} P_1(t,\tau)\, d\tau + \dfrac{\sqrt{D}}{T} \int_{t-T/2}^{T/2} P_2(t,\tau)\, d\tau & t \geq 0, \end{cases} \tag{2.13}$$

where

$$P_1(t,\tau) = \cos\left[\omega_0 t - \frac{\Delta\omega}{2T}t^2 + \frac{\Delta\omega}{T}t\tau\right],$$

$$P_2(t,\tau) = \cos\left[\omega_0(2\tau - t) + \frac{\Delta\omega}{T}\tau(\tau - t) + \frac{\Delta\omega}{2T}t^2\right].$$

The first integral can be estimated in the following way:

$$\int_a^b \cos\left[\omega_0 t - \frac{\Delta\omega}{2T}t^2 + \frac{\Delta\omega}{T}t\tau\right] d\tau = \frac{\sin\left[\omega_c t - (\Delta\omega/2T)t^2 + (\Delta\omega/T)t\tau\right]}{(\Delta\omega/T)t}\Bigg|_{\tau=a}^{\tau=b}.$$

The second integral depends on higher frequencies and, in practice, its impact on the total response can be neglected.

For $t \geq 0$ the filter response can be determined from:

$$y(t) = \frac{\sqrt{D}}{\Delta\omega t}\left\{\sin\left[\omega_0 t - \frac{\Delta\omega}{2T}t^2 + \frac{\Delta\omega}{2}t\right] - \sin\left[\omega_0 t - \frac{\Delta\omega}{2T}t^2 + \frac{\Delta\omega t}{T}\left(t - \frac{T}{2}\right)\right]\right\}. \tag{2.14}$$

The estimation of the first integral for $t < 0$ leads to similar expression; as a result, the output of the matched filter can be adequately described by the following expression:

$$y(t) = \sqrt{D}\frac{\sin \pi D\frac{t}{T}\left(1 - \frac{|t|}{T}\right)}{\pi D\frac{t}{T}}\cos\omega_0 t \qquad \text{for} \quad -T \leq t \leq T. \tag{2.15}$$

This is the autocorrelation function of the input waveform $s(t)$.

Thus, an amplitude-modulated signal with the carrier frequency f_0 is obtained at the filter output. The width of the compressed pulse is measured over the amplitude interval from $(2/\pi)\sqrt{D}$ to $\sqrt{D}$ (about 4 dB below the peak value) for the times $t = \pm 1/(2\Delta F)$; hence the total width of pulse is:

$$\Delta t = t_1 + \frac{1}{2\Delta F} - \left(t_1 - \frac{1}{2\Delta F}\right) = \frac{1}{\Delta F}. \tag{2.16}$$

This width or pulse duration is the inverse of that of the rectangular pulse. The ratio between the duration of the input signal T and the duration of the output pulse is $T/(1/\Delta F) = \Delta F T = D$. Further examination shows that the maximum value of the output signal is $\sqrt{D}$ times higher than that of the input signal, and the maximum output power in the pulse is D times higher than the input power. However, the mean power remains the same. The above analysis indicates that the principle of matching filtering as applied to the linear FM signal combines the advantages of short and long pulses. In this way, relatively high power can be transmitted in a short pulse.

The linear group delay can now be examined in more detail. This delay can be expressed as:

$$D(\omega) = -\frac{d\theta(\omega)}{d\omega} = t_1 + T\left(\frac{\omega_c - \omega}{\Delta\omega}\right), \tag{2.17}$$

where $\Delta\omega = 2\pi\Delta F$.

Knowledge of instantaneous frequency and linear delay of the filter is sufficient to perform a qualitative analysis of the amplitude transfer function and determine voltage gain for $t = t_1$.

The input signal $s(t)$ can be considered to consist an infinite number of sinusoid components the frequencies of which are defined by $\omega(t)$ for each instant of time. For

instance, for $t = t_a$ one specific sinusoid has the frequency $\omega(t_a) = \omega_0 + (\Delta\omega/T)t_a$. At the receiver input this sinusoid component is delayed with the optimum filter by the value $D(\omega)$, where $\omega = \omega(t_a)$. This sinusoid reaches the filter output after the time $t_a + D(\omega)\Big|_{\omega=\omega(t_a)}$. For a given sinusoid component the time delay from the receiver input to its output can be determined from:

$$t+D(\omega)\Big|_{\omega=\omega(t)} = t+t_1+\frac{T}{\Delta\omega}(\omega_0-\omega)\Big|_{\omega=\omega(t)} = t+t_1+\frac{T}{\Delta\omega}\left[\omega_0-\left(\omega_0+\frac{\Delta\omega}{T}t\right)\right] = t_1. \quad (2.18)$$

Therefore, all the components of the spectrum of the input signal, irrespective of their frequencies, reach the filter output at the same time t_1. Since the phase of all components is identical, the amplitude of the output signal increases for $t = t_1$. This increase in the amplitude of the output signal by a factor of $\sqrt{D}$ can be explained in the following way. The FM impulse can be expressed as the composition of N pulses each having a unit amplitude. Therefore, the width or duration of each pulse is T/N. The carrier frequency of each component pulse is constant, and approximates the linear frequency function in the corresponding interval of this component pulse (see in Fig. 2).

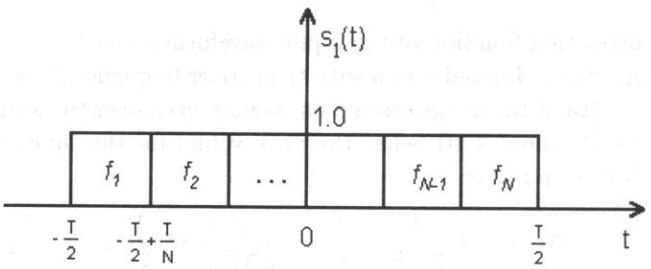

Fig. 2. The approximation of a pulse with linear FM modulation by N pulses with different carrier frequencies.

The frequency of the k-th pulse is given by:

$$f_k = f_0 - \frac{\Delta f}{2} + \frac{(2k-1)\Delta f}{2N} \qquad (k = 1, 2, ..., N), \quad (2.19)$$

which occurs for

$$t_k = -\frac{T}{2} + \frac{(2k-1)T}{2N}.$$

It is now necessary to determine the value of N to minimize the approximation error and ensure that $s'(t)$ would be the appropriate approximation of $s(t)$. The spectra of N individual component pulses can be added to obtain the overall transfer function of the chirp signal. For the frequency f_k the amplitude remains constant since the amplitude of the other components passes through zero at this frequency.

The condition for a partial superimposition of the neighbouring pulses spectra can be formulated in the following way:

$$f_{k+1} - f_k = \frac{N}{T}. \quad (2.20)$$

From the previous formulae (Eqs. (2.19) and (2.20))

$$f_{k+1} - f_k = f_0 - \frac{\Delta F}{2} + \frac{(2k+1)\Delta f}{2N} - \left[f_0 - \frac{\Delta F}{2} + \frac{(2k-1)\Delta F}{2N} \right] = \frac{\Delta F}{N} . \quad (2.21)$$

Combining (2.20) and (2.21) results in the following expression:

$$N = \sqrt{\Delta F T} = \sqrt{D} . \quad (2.22)$$

Equation (2.22) indicates that the first-order approximation of the chirp signal consists of individual components (pulses) each of duration $T/\sqrt{D}$. If $\sqrt{D}$ is not an integer $s'(t)$ cannot be implemented in practice, however, the mathematical model continues to hold.

In this study the development of the AP filter was undertaken over the frequency range from 30 MHz to 50 MHz. This is because, as mentioned in Introduction, the ultrasound imaging in this frequency range is gaining attention. Since the bandwidth available with conventional PZT ceramic transducers is not adequate the filter design described assumed that the wideband transducer characteristics could be met by using piezoelectric polymer transducers [11].

Careful analysis of the trade-off between the pulse-echo sensitivity of the superwideband PVDF transducer and the corresponding PZT transducer was carried out and it was determined that the PVDF transducer will exhibit approximately 20 dB lower sensitivity. This result was subsequently used to analyse the conditions appropriate for practical implementation of the all pass filter. The analysis resulted in selection of linear modulation range of 20 MHz and chirp signal duration of 1 μs.

As the gain of reflected echoes after compression is proportional to $\sqrt{D}$, these filter parameters will result in the $\sqrt{D} = \sqrt{1\,\mu s \cdot 20\,MHz} \cong 4.5$, close to the value of 13 dB which would greatly compensate for the 20 dB loss due to the use of PVDF transducer. It is appropriate to note that in the present analysis the influence of the tissue load was neglected. However, the practical implementation of the chirp technique would require frequency dependent attenuation effects to be taken into account. To simplify the analysis of the filter parameters, such as the compression coefficient and the duration of side lobes, it was assumed that the chirp signal amplitude was unity – this assumption does not affect the general nature of the analysis and the practical implementation of the delay line designed.

All pass filter design. The AP filter is a matched filter implementing the inverse time delay function with respect to the transmitted chirp signal. Since the chirp waveform used here has linear frequency modulation, the characteristic of the delay line needs to be linear, too. Such characteristic of the delay transfer function can be approximated using maximally flat, equiripple and least squares designs. The least-squares method was selected here as it offers an adequate compromise between the maximally flat and equiripple designs. Although the equiripple method provides a sharper roll-off characteristic than the least-squares method, it is achievable at the expense of maximally flat response. On the other hand, the maximally flat design does not provide satisfactory

results at cut-off frequencies and in the lower frequency range. The least-squares method is a compromise between these types of solutions.

Estimation and minimization of error. Optimization of the filter design requires minimization of the order of the filter and simultaneous minimization of the error between the ideal (theoretical) and achievable filter response. Another issue to be addressed in the optimization of the design is associated with the matching between the input signal and the filter. The optimum filter should be relatively insensitive to variations in the shape of the input signal.

A procedure of estimating the approximation error is presented below. The procedure allows the impact of variations in the values of the filter parameters on the linearity of the delay characteristic to be determined. In addition, the procedure makes it possible to analyse the effect of delay nonlinearity on the shape and compression of the output signal.

The total delay of a filter consisting of N cascade-connected second-order filters is given by:

$$D_a(\omega) = 4 \sum_{j=1}^{N} \frac{\alpha_j(\omega^2 + \alpha_j^2 + \beta_j^2)}{(\alpha_j^2 + \beta_j^2 - \omega^2)^2 + 4\alpha_j^2\omega^2} \,. \tag{2.23}$$

The value of error in the delay can be estimated as follows:

$$\varepsilon = \int_{\omega_1}^{\omega_2} [D_d(\omega) - D_a(\omega)]^2 \, d\omega \,, \tag{2.24}$$

where $D_d(\omega)$ is the required delay over the interval $\omega_1 \leq \omega \leq \omega_2$.

The error is minimized if the partial derivatives are zero for each variable, i.e., $d\varepsilon/d\alpha_j = 0$ and $d\varepsilon/d\beta_i = 0$. The solution of these equations yields the optimum parameters.

3. Numerical verification of the analytical results

Since analytical solution is impractical in design practice, numerical verification of the analytical results was carried out. Typically, the numerical solution will minimize the error with increasing number of approximations. The trade off here is between minimizing the error and ensuring a reasonable computation time.

There are many algorithms for numerical integration. If the integral is replaced by the equivalent rectangles the following expression is obtained:

$$\varepsilon = \Delta\omega \sum_{k=1}^{P} \left(D_{d_k} - D_{a_k}\right)^2 \,. \tag{3.1}$$

The function of Eq. (2.25) was calculated for P frequencies over the range $\omega_1 \leq \omega \leq \omega_2$, where $\Delta\omega$ is the integration interval. The first frequency to be calculated

was $\omega_1 + \Delta\omega/2$, the next one was $\omega_1 + 3\Delta\omega/2$, etc. The last frequency calculated was $\omega_2 - \Delta\omega/2$. This approach resulted in the following expression:

$$\Delta\omega = \frac{\omega_2 - \omega_1}{P}, \tag{3.2}$$

where the coefficient P is defined as $P = 4N + 5$ (N is the number of second orders filters used in the design). The higher P is the more accurately the value of the integral is determined. The initial values for the parameters α_j and β_j which usually yielded satisfactory results are given by [3]

$$\begin{aligned} \alpha_j &= \frac{\omega_2 - \omega_1}{N}, \\ \beta_j &= \omega_1 + \frac{(2j-1)(\omega_2 - \omega_1)}{2N}, \qquad j = 1, 2, ..., N. \end{aligned} \tag{3.3}$$

Prior to describing the results of numerical evaluations it may be useful to reiterate the requirements for the filter characteristics.

The purpose of the optimization procedure was to obtain a delay function with the following properties: 1) the delay function should be linear – this requirement results directly from the assumptions of the matching filtering model adopted here, 2) the total filter delay was chosen to be 1 μs over the frequency range from 30 MHz to 50 MHz and, moreover, the filter was assumed to consist of four cascade-connected sections, each with a delay of 250 ns, 3) the maxima in transfer functions of individual filters should fall between the frequency range from 30 MHz to 50 MHz.

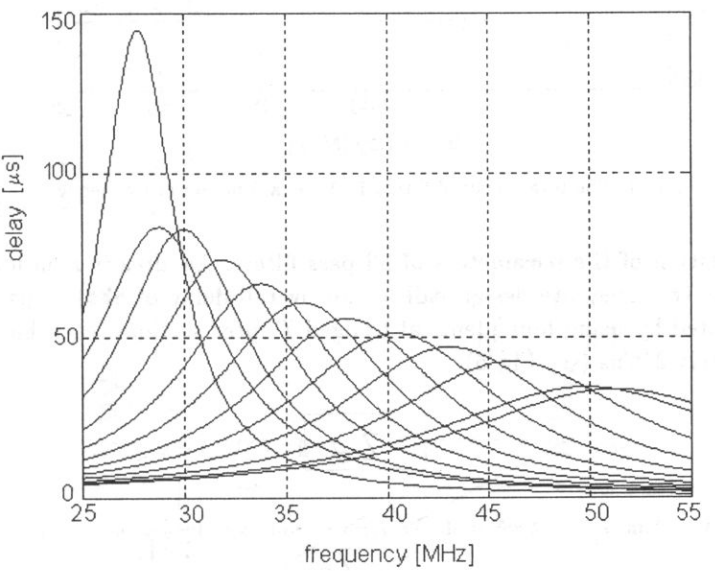

Fig. 3. The delays of filters 1 – 12 as a function of frequency.

The optimization process was performed on a Hewlett Packard 9000 series workstation using the Mathematica 2.0 software (Wolfram Research). The function Nonlinear

Curve Fitting (nonlinea.m from the Statistics package) was used. This program allows the nonlinear plot to be fitted to an arbitrary function. More specifically, Nonlinear Curve Fitting implements nonlinear approximation of a specific function using the least-squares method, such as the Levenberg-Marquardt method which minimizes chi2. The numerical analysis indicated that already for the 24-th order filter (12 second order filters), the value of the error was minimized. Further increase in the filter order did not show any significant improvement. The delays of the individual filters and the overall delay of the 24-th order filter are shown in Figs. 3 and 4. The initial and post-optimization parameter values of the filters are shown in Appendix.

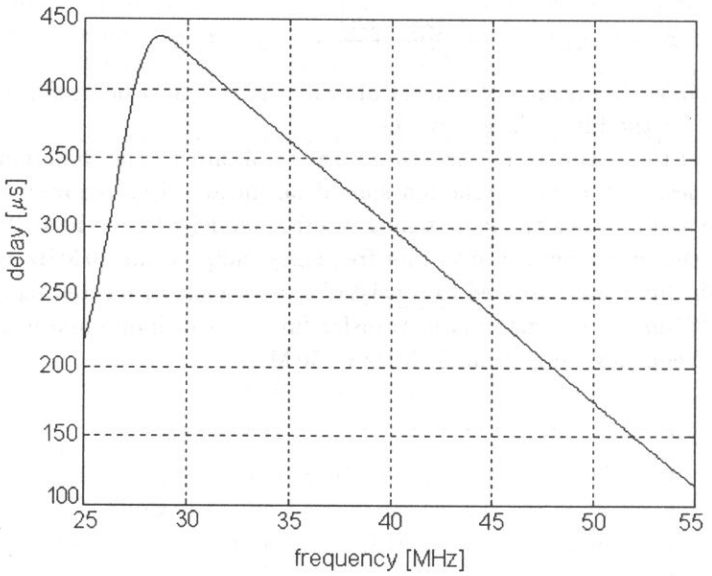

Fig. 4. The total delay of filters 1 – 12 as a function of frequency.

The calculation of the parameters of all pass filters. As already mentioned, the requirements for the adequate design call for an overall delay of about 1 μs. This delay was implemented by using four identical bridged T filter sections, each having a delay of approximately 270 ns (see Fig. 5).

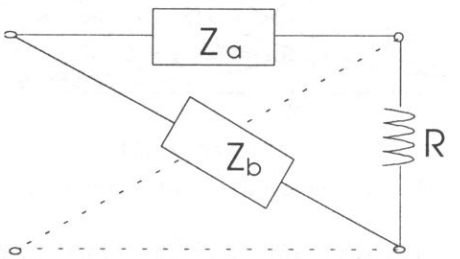

Fig. 5. Bridge-T filter with constant resistance.

For such filters the output resistance of one section of the filter R is the input resistance of its next section:

$$Z_a \, Z_b = R^2. \tag{3.4}$$

The transfer function of (3.4) has the following form:

$$H(\omega) = \frac{R - Z_a}{R + Z_a} \tag{3.5}$$

and providing that Z_a is represented by the reactance $jX(\omega)$, the filter is all-pass.

Second order Bridged T filters. For the second-order AP lattice the impedance of the anti-resonance circuit is:

$$Z_a = \frac{j\omega L}{1 - LC\omega^2} \tag{3.6}$$

and, hence, formula (3.5) becomes:

$$H(\omega) = \frac{-\omega^2 - j\omega(1/RC) + 1/LC}{-\omega^2 + j\omega(1/RC) + 1/LC}. \tag{3.7}$$

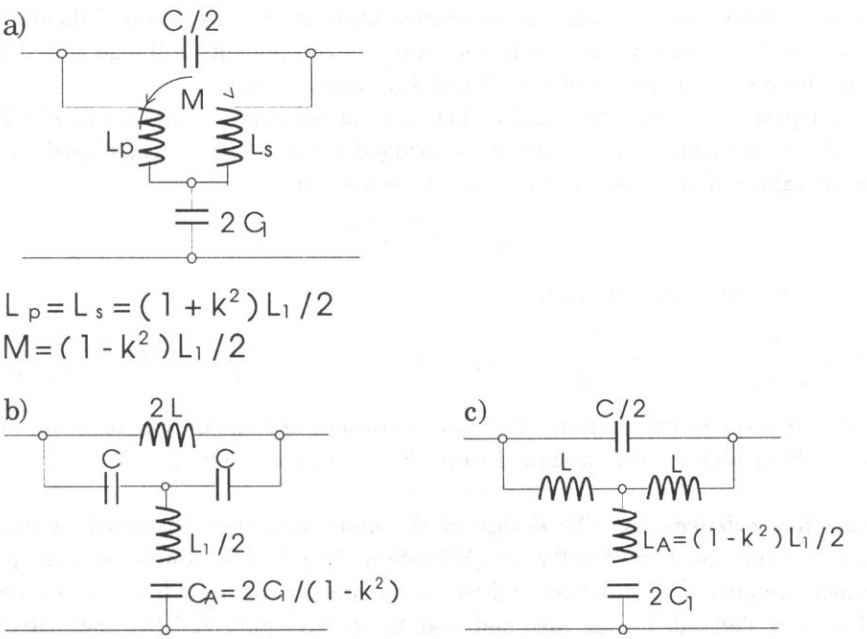

Fig. 6. The schematic diagrams of second-order bridge-T filters for $k > 1$ (a) and for $k < 1$ (b and c).

Comparison between $H(\omega)$ and $H_2(\omega)$ (Eq. (2.5)) shows that

$$\frac{1}{RC} = 2\alpha = k\overline{\omega}_0, \qquad \frac{1}{LC} = \alpha^2 + \beta^2 = \overline{\omega}^2 \tag{3.8}$$

and, hence the following expression is valid:

$$L = \frac{kR}{\overline{\omega}_0}, \qquad C = \frac{1}{k\overline{\omega}_0 R} = \frac{1}{L\overline{\omega}_0^2}. \tag{3.9}$$

The parallel resonance of L and C occur at the frequency ω_0, which with the use of (3.4) leads to:

$$Z_b = \frac{R^2\left(1 - LC\omega^2\right)}{j\omega L} = j\omega R^2 C + \frac{1}{j\omega(L/R^2)} = j\omega L_1 + \frac{1}{j\omega C_1}. \tag{3.10}$$

This is the impedance of a series circuit containing L_1 and C_1, where:

$$\begin{aligned} L_1 &= R^2 C, \\ C_1 &= L/R^2. \end{aligned} \tag{3.11}$$

The series resonance also occurs at ω_0.

The second-order bridged-T filter for the values $k > 1$ and $k < 1$ ($k = 2\alpha/\omega_0$) is shown in Fig. 6 a. When high-frequency signals are used a better choice is to use the capacitance circuit (Fig. 6 b) because higher values of inductances needed. It should be noted that the assembly and measurements of low inductances are more difficult and less accurate which would make the implementation of the filter more difficult. This is due to the fact that any variations in the values of components will lead to a deviation from the desired linear shape of the filter delay characteristic.

From equations (3.8), (3.9) and (3.11) and the schematic diagram in Fig. 7 b, the values of the elements of a second-order bridged-T filter can be calculated using the optimized values of the coefficients α and β. Specifically:

$$\omega_0 = \sqrt{\alpha^2 + \beta^2},$$

where ω_0 is the resonance frequency,

$$L = \frac{kR}{2\pi\omega_0}, \qquad C = \frac{1}{L\omega_0^2}, \qquad L_1 = R^2 C, \qquad C_1 = \frac{L}{R^2}, \qquad C_A = \frac{2C_1}{1 - k^2}.$$

In the subsequent calculations the input resistance and the output resistance of each bridged T filter section were assumed to be $R_{\text{in}} = R_{\text{out}} = 50\,\text{Ohms}$.

Delay line calculations. The design of the delay line was conducted by computer simulation using the Pspice software (MicroSim Corp.). The source of a chirp signal with linear frequency modulation and the delay line circuit built from the elements R, L and C were defined. It was assumed that the chirp signal had the centre frequency $f_0 = 40\,\text{MHz}$, $\Delta F = 20\,\text{MHz}$, the pulse duration $T = 1080\,\text{ns}$ (four filter section were assumed each having a $T = 270\,\text{ns}$).

As mentioned previously in the computer simulation a 24-th order filter section consisting of 12 second-order cascaded filters sections was investigated. The values of the discrete R, L, C elements were determined from the calculations outlined above. Figure 7 a, b shows the frequency responses of the filter obtained for different delays. As

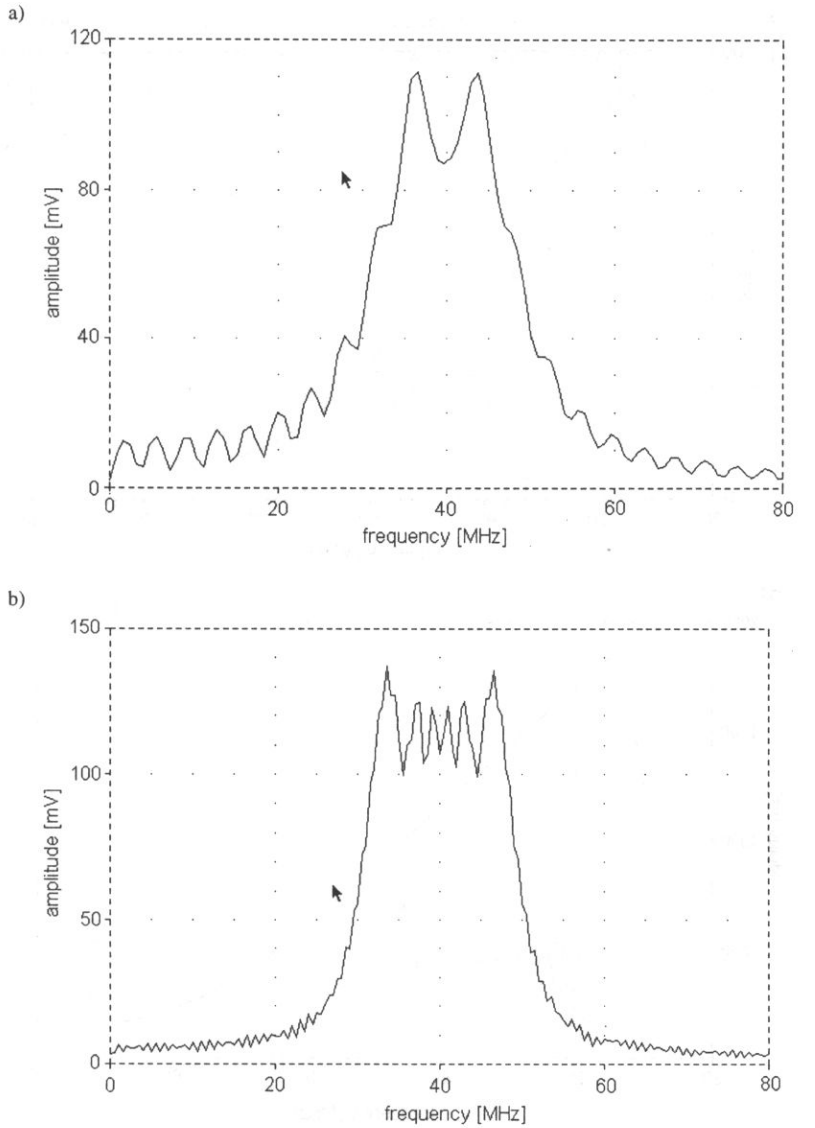

Fig. 7. Spectral amplitude of the rectangular chirp signal (a) $T = 270\,\text{ns}$ (for one filter section), (b) $T = 1080\,\text{ns}$ (for four filter sections).

expected the frequency responses show Fresnel inequalities which depend on the pulse length T (for the constant ΔF values). As the value of T increases these inequalities become smaller. A sinusoidal signal with a normalized amplitude over the frequency range between 25 and 55 MHz (this bandwidth was by $+/-5\,\text{MHz}$ wider than the modulation bandwidth) was used to determine the frequency response of the delay line model. The frequency response is the most important characteristic of the filter system, determining the quality of the matching of the model to the chirp signal.

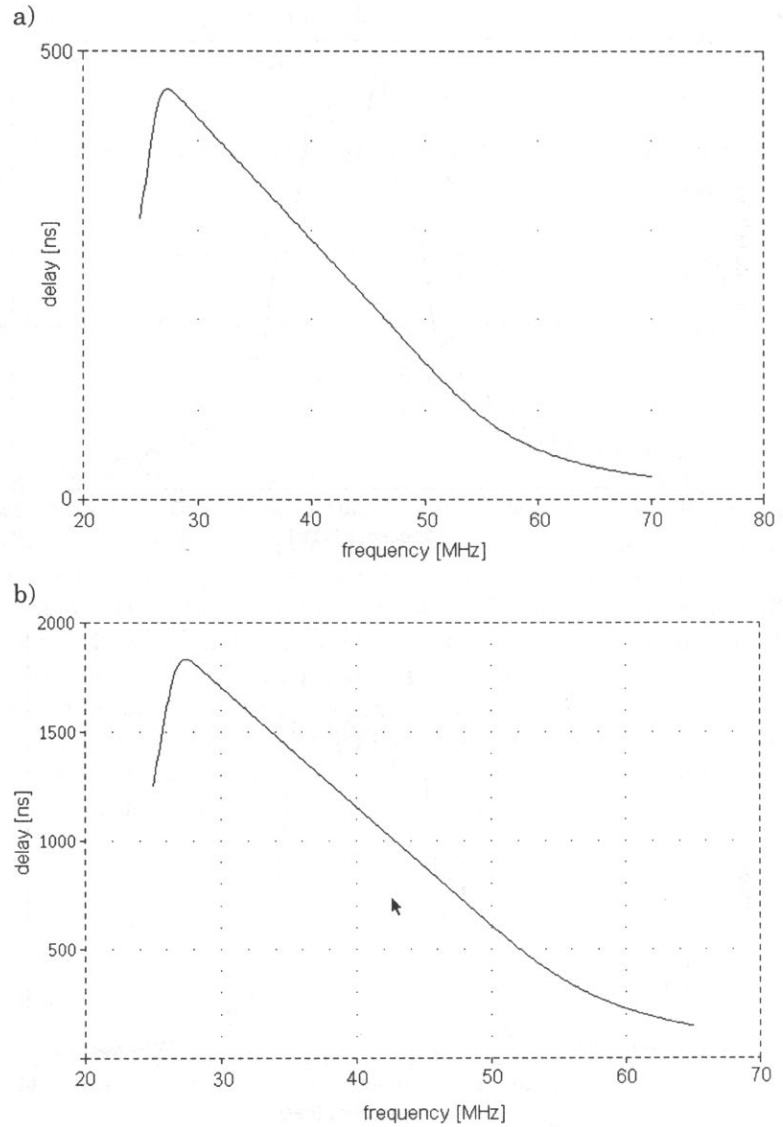

Fig. 8. The delay characteristic as a function of the frequency of the filter designed: (a) for one section of the filter, (b) for four sections of the filter.

The plots in Fig. 8 a, b show the delay characteristics of the chirp signal obtained for one filter section and four identical cascaded filter sections. The overall delay versus frequency, the achievable delay range for frequencies between 30 and 50 MHz and the initial and final chirp signal delays can be read from these plots. It can also be noted that the transfer function of an ideal, optimized filter consisting of one or more sections is linear in nature. This confirms that the filter design procedure presented here is adequately matched to the chirp signal.

Time response. As a next step in the numerical design the time response of the filter designed was investigated. Figure 9 a, b show pulses after compression for one and three series-connected filter sections.

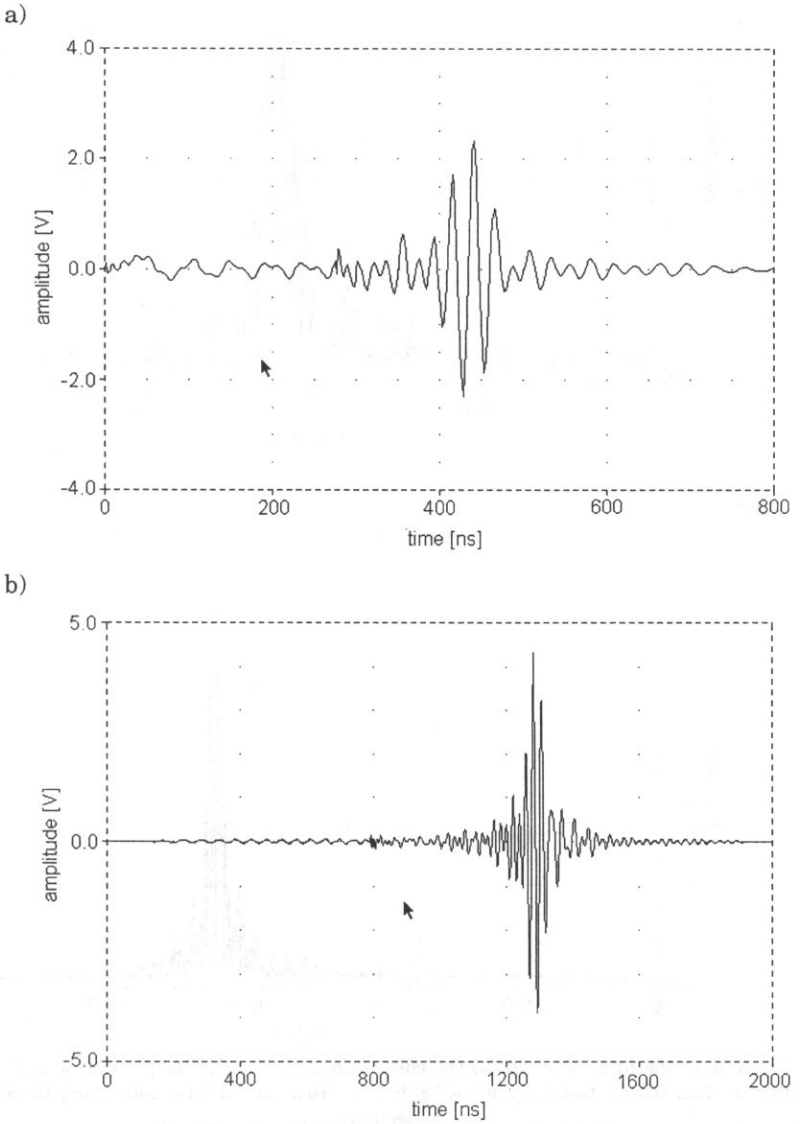

Fig. 9. Filter response to the chirp signal: (a) for the chirp signal with $T = 270$ ns and one filter section, (b) for the chirp signal with $T = 810$ ns and a filter containing three cascaded sections.

Given the very complex analysis of a system built from four sections, with the computer hardware configuration in hand the programme PSpice was able to perform a correct analysis of the transient response only for the filter consisting of up to three sections (72-nd order).

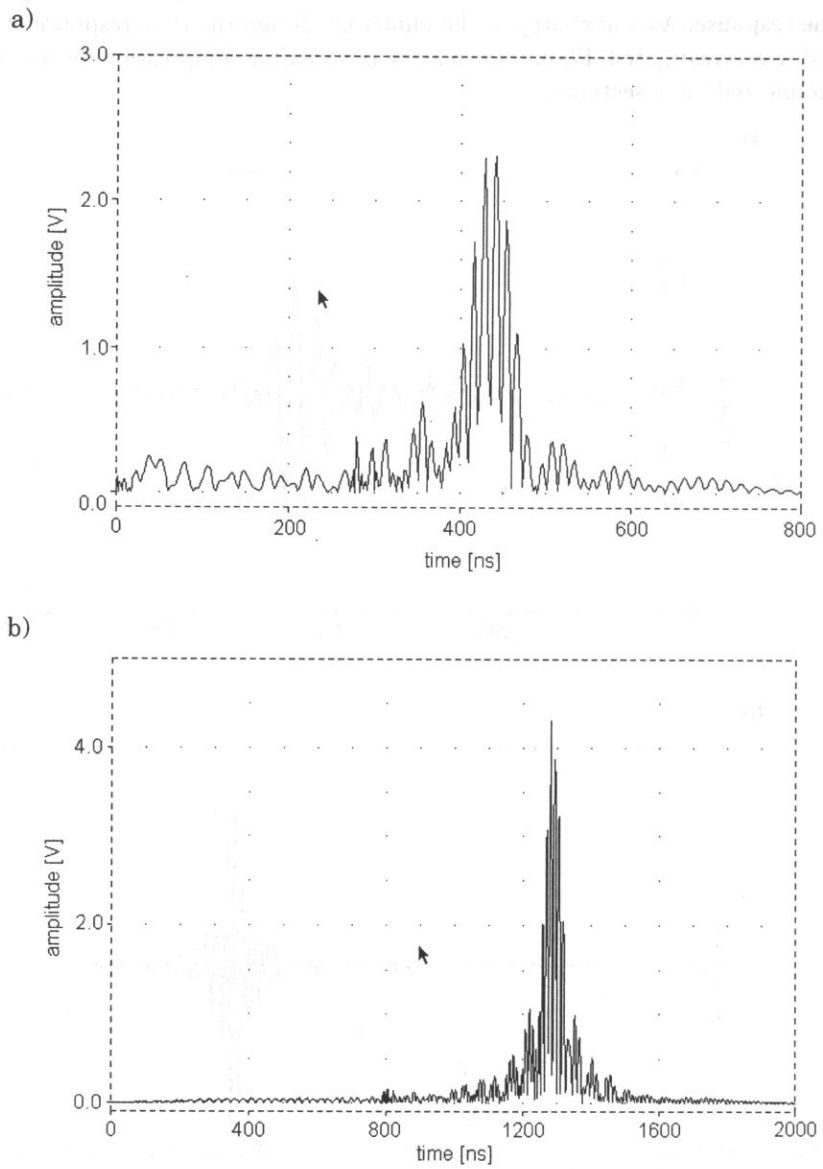

Fig. 10. Envelope of the filter response to the chirp signal: (a) for the chirp signal with $T = 270$ ns and one filter section, (b) for the chirp signal with $T = 810$ ns and a filter containing three cascaded sections.

Figure 10 a, b presents the transient response plots comparable to those presented in Fig. 9 a, b. The plots show the echo behaviour after compression. The calculated parameters of signal compression are listed in Table 1.

The results of the computer simulation presented above verify the analytical analysis and indicate the feasibility of the optimization of the matched filter.

Table 1.

	1 section ($T = 270$ ns)	2 sections ($T = 540$ ns)	3 sections ($T = 810$ ns)
Signal amplitude after compression $[A/A_0]$	2.35	2.90	4.20
Pulse width (main lobe) [ns]	~100	~110	~100

Sensitivity analysis. An analysis of the effect of the tolerance of the filter elements on the delay and transient response characteristics of the delay line was also performed.

a)

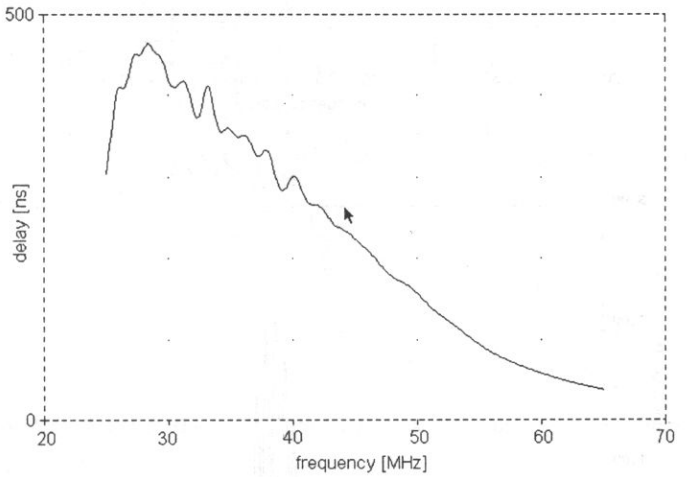

b)

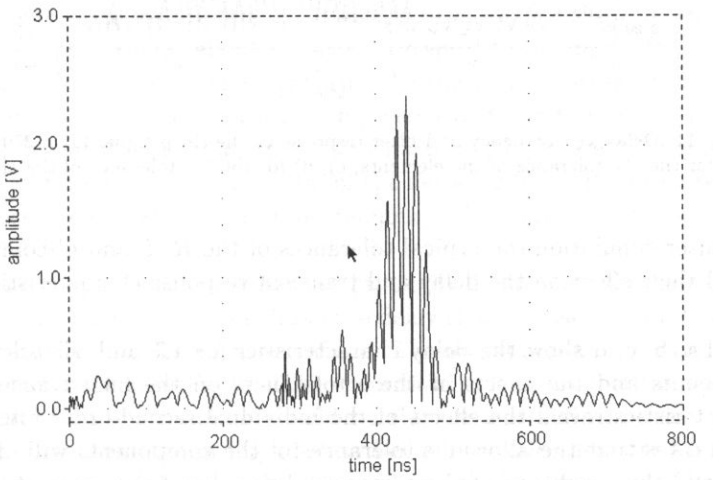

[Fig. 11 a, b]

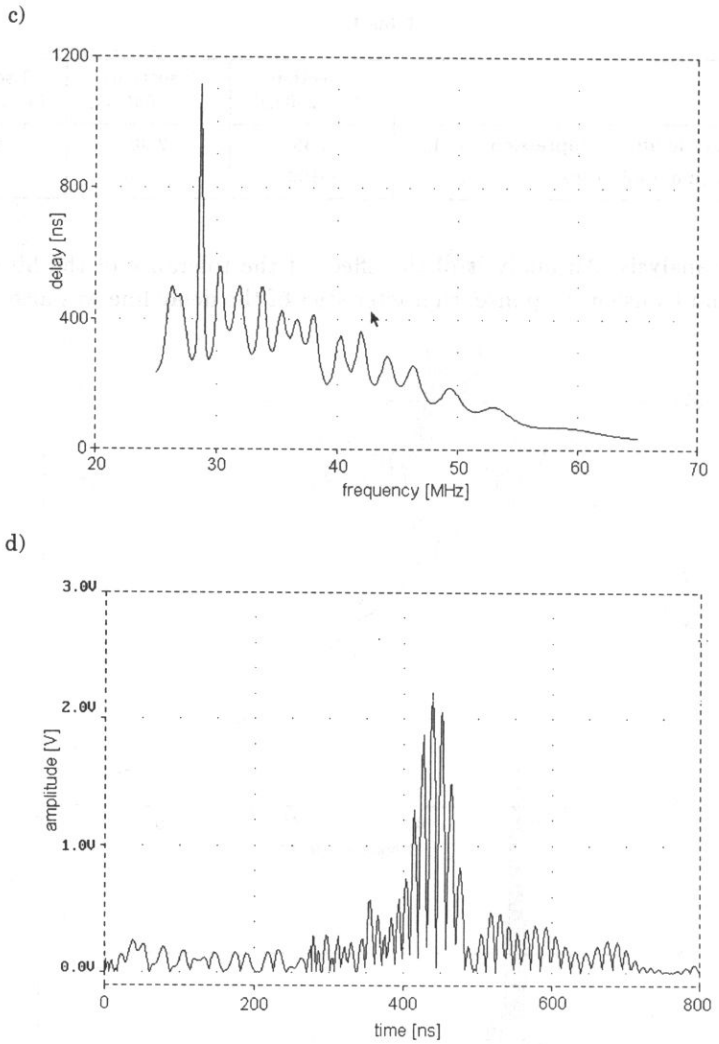

Fig. 11. Delay vs. frequency and filter response to the chirp signal ($T = 270$ ns): a), b) for the 1% tolerance of the elements, c), d) for the 5% tolerance of the elements.

In the computer simulation the typical tolerances of the R, L and C components were assumed and their effect on the delay and transient response characteristics was determined.

Figure 11 a, b, c, d show the delay characteristics for 1% and 5% tolerances of the filter components and the effects of these tolerances on the final transient response. Delay characteristics reveal the effects of the individual second-order filters. Transient response indicates that the allowable tolerances of the components will also affect (although slightly) the amplitude of the compressed signal and the range of the side lobes of the signal.

4. The implementation and experimental verification of the delay filter

One section of the 24-th order all pass filter was designed, constructed and characterized. The design was implemented using bridge-T type filter shown in Fig. 6 b. This implementation offered the most advantageous values of L and C components.

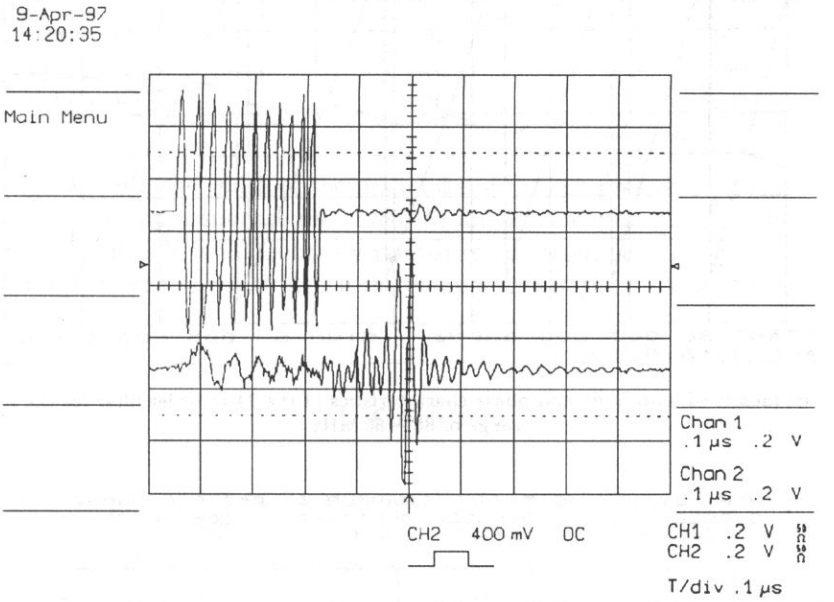

Fig. 12. The chirp signal at the input – (lower plot) and the filter response (upper plot).

The Arbitrary Function Generator LeCroy 9109 was used to generate the chirp signal. This chirp signal was fed to the input of the delay line (24-th order filter). Figure 12 presents the input chirp signal and the response of a single section of the delay line. The maximum output delay is about 250 ns with respect to the input (for a frequency of 40 MHz), which is in excellent agreement with the theoretical assumptions. The output signal from the single section is clearly compressed and has the maximum amplitude amplified by a factor of more than two than that of the input signal. Figure 13 shows the amplitude and phase transfer function of the designed filter. It can be seen that the amplitude varies slightly as a function of frequency; this amplitude variation is due to the losses in the design.

However, the properties of the filter are primarily determined by the delay transfer function or characteristic. Figure 14 shows the delay characteristic for one section of the filter versus frequency for the chirp waveform. The initial and final delays of the filter can also be determined from Fig. 14. The theoretical calculations of the delay transfer function indicate that the function should be that of a straight line (see Fig. 8 a, b), however, the results presented in Fig. 14 show behaviour which deviates somewhat from the expected straight line dependency. This is because the experimentally determined delay of the filter section was about 270 ns versus 250 ns used in computer simulations.

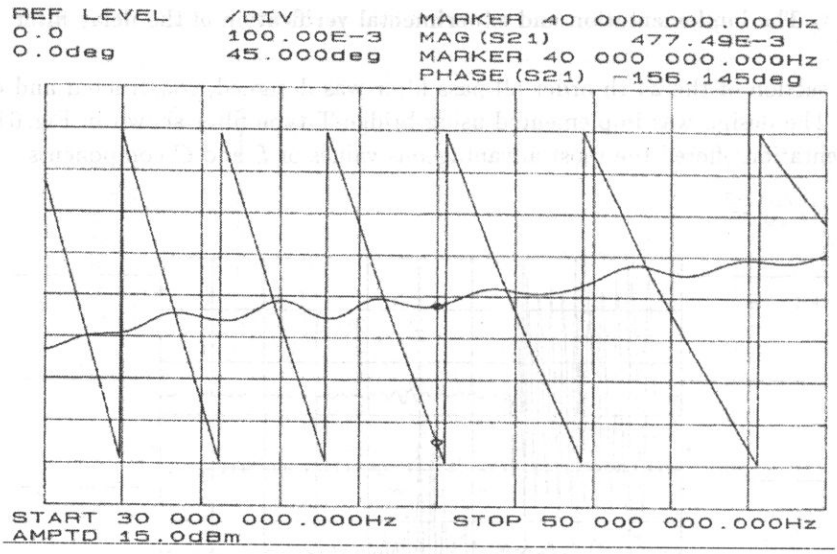

Fig. 13. The measured amplitude and phase characteristics of the 24-th order filter for the frequency range of 30 – 50 MHz.

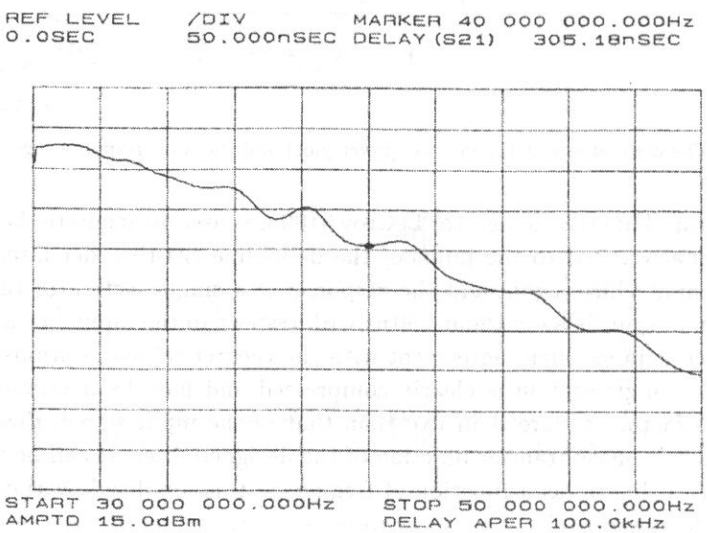

Fig. 14. The measured delay characteristic of the 24-th order filter.

Also, in the computer simulation of the filter section, the delay filter was implemented with ideal capacitance and inductance elements. Thus, the numerical model did not include the effects of parasitic or stray capacitances and assumed lossless L and C elements. Also, the existence of ripples in the characteristics can be traced to nonideal components and their tolerances and the achievable accuracy in filter tuning.

Table 2 compares key parameters of the all pass filter designed. The data of Table 2 indicate that the predicted and measured parameters are in very good agreement.

Table 2.

	Main lobe amplitude [$A/A0$]	Main lobe width [ns]
Mathematical model	2.32	100
Computer simulation	2.35	~100
Filter prototype	2.20	~100

In practice, both the width of the main lobe of the compressed signal and the signal amplitude after compression are preserved. As already mentioned, the slight drop in the value of the amplitude is undoubtedly related to the tolerancies of the filter prototype components and accuracy with which the components of the filter were tuned.

5. Conclusions

The primary goal of this work was to investigate a possibility of using chirp waveforms in very high frequency ultrasound medical imaging to increase range resolution and concurrently maximize penetration depth.

A mathematical analysis was conducted for the chirp waveform and the model of a matched all pass filter at the receiver input which appropriately delayed this signal. The analysis allowed the parameters of the filter to be optimized. The filter model calculated in this way was subsequently analysed by computer simulations which verified the results of the mathematical approach. The theoretical considerations were concerned with both a single filter section and the matched 96-th order all pass filter for chirp signal of $1\,\mu s$ duration in the frequency range $30\,MHz - 50\,MHz$. A prototype of 24-th order filter was constructed to verify the results of analytical and numerical methods. The filter was investigated in terms of the delay characteristics. Also, the parameters of the chirp signal after compression at the filter output were measured. Excellent agreement was observed between the theoretical predictions and experimental data.

Although the experimental results of this work indicate that the construction of the matched 96-th order all pass filter for chirp signal is feasible, the experimental evaluation of the 24-th order all pass filter was performed using electrical signal only, thus neglecting the effects associated with the electromechanical energy conversion. Continuation of this work will need to include design and optimization of superwide bandwidth transducers so the filter input will receive the echoes converted into the electrical waveforms by the ultrasound transducer. Accordingly, the next stage of this work will include determination of the transfer function of wideband PVDF transducers. The overall performance of the matched filter including degree of compression will most likely depend on the pulse-echo characteristics of those transducers.

Appendix

The delay of the 24-th order AP filtere is given by:

$$D_a(\omega) = 4\sum_{j=1}^{12} \frac{\alpha_j(\omega^2 + \alpha_j^2 + \beta_j^2}{(\alpha_j^2 + \beta_j^2 - \omega^2)^2 + 4\alpha_j^2\omega^2} .$$

Table 3. Starting values and the computed ones of the parameters α_j and β_j.

Starting values α and β for AP filter	Values of α and β after optimization
$\alpha_1 = \alpha_2 = ... = \alpha_{12} = 10.474e6$ [Hz]	$\alpha_1 = 24.211e6$ [Hz]; $\alpha_2 = 13.824e6$ [Hz]; $\alpha_3 = 24.024e6$ [Hz]; $\alpha_4 = 27.219e6$ [Hz]; $\alpha_5 = 30.273e6$ [Hz]; $\alpha_6 = 33.028e6$ [Hz]; $\alpha_7 = 36.169e6$ [Hz]; $\alpha_8 = 39.357e6$ [Hz]; $\alpha_9 = 43.012e6$ [Hz]; $\alpha_{10} = 47.600e6$ [Hz]; $\alpha_{11} = 59.969e6$ [Hz]; $\alpha_{12} = 58.758e6$ [Hz];
$\beta_1 = 193.729e6$ [Hz]; $\beta_2 = 204.204e6$ [Hz]; $\beta_3 = 214.678e6$ [Hz]; $\beta_4 = 225.145e6$ [Hz]; $\beta_5 = 235.619e6$ [Hz]; $\beta_6 = 246.093e6$ [Hz]; $\beta_7 = 256.561e6$ [Hz]; $\beta_8 = 267.035e6$ [Hz]; $\beta_9 = 277.503e6$ [Hz]; $\beta_{10} = 287.977e6$ [Hz]; $\beta_{11} = 298.451e6$ [Hz]; $\beta_{12} = 308.925e6$ [Hz];	$\beta_1 = 188.40e6$ [Hz]; $\beta_2 = 174.42e6$ [Hz]; $\beta_3 = 180.68e6$ [Hz]; $\beta_4 = 200.34e6$ [Hz]; $\beta_5 = 212.34e6$ [Hz]; $\beta_6 = 225.10e6$ [Hz]; $\beta_7 = 238.88e6$ [Hz]; $\beta_8 = 253.95e6$ [Hz]; $\beta_9 = 270.62e6$ [Hz]; $\beta_{10} = 289.64e6$ [Hz]; $\beta_{11} = 321.69e6$ [Hz]; $\beta_{12} = 312.93e6$ [Hz];

References

[1] P. ALTMEYER, S. EL-GAMMAL, K. HOFFMAN [Eds.], *Ultrasound in dermatology*, Springer-Verlag, Berlin 1992.

[2] M. BERSON, L. VAILLANT, F. PATAT, L. POURCELOT, *High resolution real time ultrasonic scanner*, Ultrasound Med. and Biol., **18**, 5, 471–478 (1992).

[3] H.J. BLINCHIKOFF, A.I. ZVEREW, *Filtering in the time and frequency domains*, J. Willey & Sons, New York 1976.

[4] J.L. EAVES and E.K. REEDY [Eds.], *Principles of modern radar*, Van Nostrand, Reihold, New York 1987.

[5] G. FEUILLARD, M. LETHIECQ, L. TESSIER, F. PATAT, M. BERSON, *High resolution B scan imaging of the skin using a 50 MHz P(VDF-TrFe)- based ultrasonic transducer*, European J. Ultrasound, **1**, 2, 183–189 (1994).

[6] J. FILIPIAK, *Zagadnienia syntezy podzespołów z akustyczną falą powierzchniową do obróbki sygnałów złożonych typu chirp* [in Polish], WAT, Warszawa 1993.

[7] H.S. FREW, R.A. GIBLIN, *The choice of ultrasound frequency for skin blood flow investigation*, Bioeng. Skin, **1**, 193–205 (1985).

[8] A. HOSS, H. ERMERT, S. EL-GAMMAL, P. ALTMEYER, *Signal processing in high-frequency broadband imaging systems for dermatologic application*, [in:] Acoustical Imaging, vol. 19, H. ERMERT and H.P. HARJES [Eds.], Plenum Press, New York, 243–249, 1992.

[9] J.R. KLAUDER, A.C. PRICE, S. DARLINGTON, W.J. ALBERSHEIM, *The theory and design of chirp radars*, The Bell System Technical Journal, **39**, 4 (1960).

[10] P.A. LEWIN, *New ultrasound safety indicators and their clinical implications*, Ultrasonografia Polska, **7**, 1, 7–14 (1997).

[11] P.A. LEWIN and M.E. SCHAFER, *Wideband piezoelectric polymer acoustic sources*, IEEE Trans. UFFC, **35**, 175–184 (1988).

[12] G.K. LEWIS, *Chirped PVDF Transducers for Medical Ultrasound Imaging*, Proceeding of Ultrasonic Symposium 1987.

[13] A. NOWICKI, J. LIWSKI, W. SECOMSKI, P. KARŁOWICZ, J. LITNIEWSKI and WYTRYKOWSKI, *Ultrasound system for tissue microsonography*, Proc. X Symp. on Hydroacoustics, 145–150, Gdynia 1993.

[14] M.I. SKOLNIK, *Introduction to Radar Systems*, McGrow-Hill Book Comp. New York 1962.

[15] T. YANO, H. FUKUITA, S. UENO, A. FUKUMOTO, 40 MHz *ultrasound diagnostic system for dermatologic examination*, IEEE 1987 Ultrasonic Symposium Proceeding, 857–878, 1987.